ROYAL SOCIETY OF CHEMISTRY

## PAPER

Check for updates

# Elementary kinetics of nitrogen electroreduction to ammonia on late transition metals†

Gholamreza Rostamikia,[a] Sharad Maheshwari[b] and Michael J. Janik (ID) *[b]

Developing small scale nitrogen to ammonia conversion devices could greatly help sustainable agriculture. The lack of effective cathode materials for reduction of nitrogen to ammonia puts a major limitation on developing small scale electrochemical ammonia production devices that can operate at low pressures and temperatures. In this study, the electrochemical nitrogen reduction reaction (NRR) mechanism is investigated over late transition metals. Activation barriers for possible rate limiting steps are calculated using density functional theory (DFT) methods and are converted to potential dependent electrochemical barriers. Associative and dissociative paths are evaluated and the associative path shows lower barriers on all metals considered at NRR potentials. Brønsted–Evans–Polanyi (BEP) relationships are evaluated for rate limiting steps and a "kinetic volcano" is demonstrated for catalyst optimization. Rhodium (Rh) and iron (Fe) appear to have the lowest kinetic barriers to convert $N_2$ to $NH_3$. A large over-potential, however, is required to convert nitrogen to ammonia over all the surfaces considered. The hydrogen evolution reaction (HER) has a lower activation barrier compared to NRR, demonstrating the kinetic selectivity challenge.
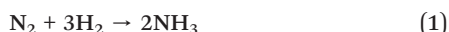
## 1. Introduction

The Haber–Bosch process has enabled our world to feed 7 billion people.[1] Invention of this process enabled mass production of ammonia, a fertilizer ingredient that helped population growth to current levels. Although the Haber–Bosch process is well optimized, it requires high pressure and temperature and cannot be used for small scale ammonia production. Hydrogen gas and nitrogen react at high pressures and temperatures over an iron catalyst to produce ammonia:

$$N_2 + 3H_2 \rightarrow 2NH_3 \qquad (1)$$

This process requires a large infrastructure and capital investment. Development of small scale ammonia production devices, powered by renewable sources and operating at ambient pressure and temperature, can greatly help sustainable agriculture.

Electrochemical reduction of nitrogen to ammonia has gained interest in the past few decades.[2,3] In this process, nitrogen can reduce to ammonia in an aqueous environment at the cathode using 6 electrons and water as the source of hydrogen:

$$N_2 + 6H_2O + 6e^- \rightarrow 2NH_3 + 6OH^- \qquad (2)$$

The poor performance of the cathode electrocatalyst puts a major limitation on practicality of these devices. Multiple recent studies point out that, due to low catalytic activity, large overpotentials are required to reduce nitrogen to ammonia.[4,5] The undesirable hydrogen evolution reaction (HER) also greatly reduces the Faradaic efficiency to less than 10% at ambient conditions:[4,6–8]

$$2H^+ + 2e^- + * \rightarrow H_2 + * \qquad (3)$$
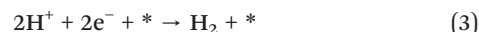
Multiple materials[9,10] including metals, alloys,[11] enzymes[12] and metal nitrides[13] have been tested for NRR, however, all tested materials suffer from low selectivity and activity for this reaction. Lan *et al.* tested platinum for the reduction reaction and observed a large overpotential and a Faradaic efficiency below 1% in the presence of water; 99% of the electricity was used to produce hydrogen rather than ammonia.[6] Qing *et al.* reported a 2.1% faradaic efficiency at 220 °C using platinum electrodes.[8] Cook *et al.* tested ruthenium for this reaction and reported an extremely low faradaic efficiency of 0.0015%.[14] Kordali *et al.* also tested ruthenium and reported a faradaic efficiency less than 1% for nitrogen reduction.[15] Iron has been tested at ambient pressure, showing low current efficiencies.[16] Licht *et al.* used an $Fe_2O_3$

[a] *University of North Carolina – Wilmington, Department of Chemistry and Biochemistry, Wilmington, NC, USA*
[b] *The Pennsylvania State University, Department of Chemical Engineering, University Park, PA, USA. E-mail: mjanik@psu.edu; Fax: +(814)865 7846; Tel: +(814)863 9366*
† Electronic supplementary information (ESI) available. See DOI: 10.1039/c8cy01845f

cathode catalyst in a molten electrolyte cell and reported 35% electrolysis efficiency, though requiring an elevated temperature of around 200 °C.[7]

Low NRR activity and selectivity makes experimental determination of mechanism, or even relative activity of different catalysts, difficult to determine. NRR is a complex reaction that goes through at least 6 elementary steps. Due to the complexity of NRR and experimental limitations to identify reaction intermediates, electronic structure calculations have been used to help explain the reaction mechanism and limiting steps.[4,5,17–19] Montoya *et al.* used DFT calculations of elementary step reaction free energies to determine possible rate limiting steps.[4] Their findings illustrate that late transition metal catalysts such as platinum, palladium, nickel, cobalt and ruthenium are limited by the reductive adsorption of nitrogen on the surface

$$N_2(gas) + * + H^+(aq) + e^- \rightarrow N_2H* \qquad (4)$$
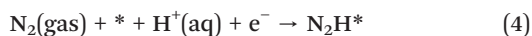
where * represents a bare catalyst surface. They predict that more strongly binding transition metals are limited by the hydrogenation of the NH* species on the surface to form $NH_2^*$

$$NH* + H^+ + e^- \rightarrow NH_2^* \qquad (5)$$
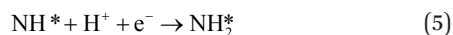
These findings are solely based on elementary step thermodynamics, embedding the assumption that activation barriers of these reactions correlate with the reaction energies across different metals.

Herein, we use density functional theory (DFT) methods to explicitly evaluate the elementary reaction barriers of NRR on late transition metal surfaces. A (111) surface is used to model the reaction steps on FCC metals with comparison to barriers on iron (110 surface) and ruthenium (0001) surfaces. Activation energies of the initial reductive adsorption of nitrogen are calculated and compared with nitrogen dissociation barriers. We then consider the barriers to reactions (4) and (5) above, as these were proposed to be the rate limiting steps across many metals based on elementary step reaction energies,[4,5] and had the highest DFT-calculated barriers on the Fe(100) surface.[20] We evaluate the reliability of Brønsted–Evans–Polanyi (BEP) relationships that correlate activation barriers with corresponding reaction energies across fcc (111) surfaces. Though these correlations only roughly hold, they are used to show a "kinetic volcano" in which the trade-off between strong and weak surface–nitrogen binding is seen to optimize the elementary reaction kinetics. NRR barriers are compared with HER barriers to quantify the challenge in developing a selective NRR electrocatalyst.

## 2. Computational methods

All calculations were performed using the *ab initio* total-energy and molecular-dynamics Vienna *ab initio* simulation program (VASP) developed at the Institute for Material Phys-

ics at the University of Vienna.[21–23] The electronic structure was represented using the Perdew-Wang[24] form of the generalized gradient approximation (GGA) and the projector augmented wave method. Exchange and correlation energies of iron were calculated using the Perdew, Burke, and Ernzerhof (PBE) functional[25] described by GGA. A cut off energy of 450 eV was used for the plane wave basis set. A $5 \times 5 \times 1$ Monkhorst–Pack mesh was used for sampling of the first Brillouin zone.[26] For all metals, other than iron and nickel, calculations were spin-restricted. During structural optimizations, the forces on all atoms were reduced to less than 0.05 eV Å$^{-1}$. The climbing image nudged elastic band (CI-NEB) method was used to isolate the transition states.[27,28] In each transition state search, four images were used between the initial and final state. An image with highest energy and an absolute tangential force of less than 0.05 eV Å$^{-1}$ was identified as the transition state and was confirmed to have a single imaginary harmonic vibrational frequency. The harmonic oscillator approximation was used to calculate vibrational modes and to determine the zero-point vibrational frequency (ZPVE) and vibrational entropic corrections to the total energy. Surfaces of M(111) metals (M = Pt, Pd, Ni, Rh, Cu and Ir), Ru(0001) and Fe(110) were modeled using $3 \times 3$ four layer slabs with the bottom two layers constrained and top two layers allowed to relax. A 15 Å vacuum space was inserted between the periodic surface slabs and dipole corrections were added in the surface normal direction to remove unphysical periodic dipole interactions.

To evaluate the activation barrier for the initial reductive adsorption of nitrogen (eqn (4)), the barrier of the non-electrochemical hydrogenation step was calculated:

$$N_2(gas) + H_2O + H* \rightarrow N_2H* + H_2O \qquad (6)$$

A Heyrovsky-like mechanism was assumed for the proton transfer where the reaction is assisted with a water molecule. Barriers are referenced to gas phase $N_2$, as molecular nitrogen binds very weakly to the majority (other than Fe) surfaces considered herein. The energy of the transition state for reaction (6) was referenced to the free energy of gas phase nitrogen and aqueous phase water at 298 K.

$$Ga_1 = G_{TS} - G_{H*} - G_{H_2O(aq)} - G_{N_2(gas)} \qquad (7)$$

This non-electrochemical activation barrier was converted to the potential dependent electrochemical barrier of reaction (4) using our previously developed method:[29]

$$Ga_1(U) = Ga_1(U_0) + \beta(U - U_0) \qquad (8)$$

where $Ga_1(U)$ is the activation barrier of reaction (4) at any given potential ($U$), $\beta$ is the symmetry factor and $U_0$ is the equilibrium potential for adsorption/desorption of surface hydrogen (H*).

For most electrochemical systems, $\beta$ falls in the range of 0.3–0.7.[30] An approximate value of $\beta = 0.5$ is used in all calculations to estimate the potential dependent activation barriers.

This journal is © The Royal Society of Chemistry 2019

*Catal. Sci. Technol.*, 2019, **9**, 174–181 | 175

Similarly, the activation barrier ($Ga_2$) for the reductive hydrogenation of NH* species (reaction (5)) is calculated using the non-electrochemical barrier for:

$$NH^* + H_2O + H^* \rightarrow NH_2^* + H_2O \qquad (9)$$
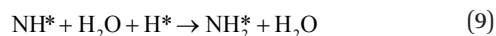
and is converted to an electrochemical barrier equivalently to eqn (8).

To confirm the dominant reaction path, the activation barrier of $N_2$ dissociation is calculated:

$$N_2^* \rightarrow 2N^* \qquad (10)$$
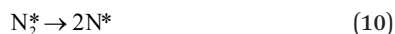
The transition state energy is referenced to the free energy of nitrogen in the gas phase

$$Ga_3 = G_{TS} - G_* - G_{N_2(gas)} \qquad (11)$$

The hydrogen evolution reaction (reaction (3)) can be written as following two elementary steps:

$$H^+ + e^- + * \rightarrow H^* \qquad (12)$$

$$2H^* \rightarrow H_2(gas) + * \qquad (13)$$

where reaction (12) represents the Volmer step of proton adsorption to the surface. In this study, the activation barrier for proton transfer to the surface is approximated with the barrier for water assisted transfer of H* from one site to another as in reaction (14):

$$H^* + H_2O \rightarrow H_2O + H^* \qquad (14)$$

The activation barrier is then made potential dependent equivalently to eqn (8). Similarly, the activation barrier for the Tafel step (eqn (13)) is also calculated using VASP on a $3 \times 3$ surface cell

$$2H^* \rightarrow H_2(gas) + * \qquad (15)$$

where the initial state has a surface coverage of 2/9 monolayer (ML) of hydrogen. Increasing the surface coverage of species will change the binding energy of surface species and activation barriers. All calculations in this study were performed in $3 \times 3$ surface cells which represents a relatively low surface coverage of adsorbates on the surface. This allows for the comparison between NRR and HER across metals at their respective low coverage limits. Coverage effects may be expected to mitigate the differences among metals without altering the trends in relative reactivity.[31] The presence of surface adsorbed OH* and O* species was not considered, as we have assumed these species would be reduced off the surface at any potential where $N_2$ reduction was favorable.

# 3. Results and discussion

Density functional theory calculations are used to determine the elementary barriers in the NRR reaction on late transition metal surfaces. We first consider the relative barriers for $N_2$ dissociation and $N_2$ reduction to $N_2H^*$ to demonstrate that the associative path is dominant (section 3.1). In section 3.2, we report the barriers for NH* reduction to $NH_2^*$, and compare these barriers with $N_2H^*$ formation barriers to illustrate the trade-offs in elementary step kinetics in optimizing NRR catalysts. We then compare the elementary barriers for NRR with those for HER on the same metals calculated with the same methods in order to quantify the NRR selectivity challenge based on elementary kinetics (section 3.3).

### 3.1. Elementary barriers for initial associative and dissociative paths

Little experimental evidence is available regarding the reaction path and limiting steps of electrochemical nitrogen reduction. However, DFT reaction free energies suggest that the initial step of reductive adsorption of $N_2$ (eqn (4)) is limiting across most late transition metals and the associative reaction path is favorable. Based on the elementary step thermodynamic data, it is proposed that the $N_2$ molecule will not initially dissociate on the surface, instead hydrogenating to form $N_2H^*$.[4] As this conclusion has been reached without availability of DFT barriers, we first assess the relative barriers of initial dissociation and reduction of $N_2$ to $N_2H^*$. Fig. 1 illustrates the configuration of reactants, products and transition states for $N_2$ reduction on the Pt(111) surface. Images of all structures on all surfaces considered are included in the ESI.† $N_2H^*$ has a strong preference to bind parallel to the surface, with an "end-on" adsorption 0.3 eV higher in energy on Pt(111) and 0.75 eV higher on Fe(110). We have therefore chosen to orient $N_2$ parallel to the surface in the initial state to facilitate location of the optimal parallel orientation of the $N_2$–H* formation transition state. $N_2$ binds very weakly to all non-Fe surfaces considered (and adsorbs parallel on Fe surfaces), and our activation barriers are reported with reference to the gas phase $N_2$ energy due to expected low coverage of adsorbed molecular $N_2$. The energy of the initial $N_2^*$ state, therefore, does not enter into the reported results. The potential dependent activation barriers for $N_2$ reductive adsorption, across low-index surfaces of a series of late transition metals, were calculated at 0 V-RHE using eqn (8) and are compared with $N_2$ dissociation barriers.

Fig. 2 plots $N_2$ reduction and dissociation barriers against the N* binding energy (relative to gas phase 1/2 $N_2$). As the $N_2H^*$ binding energy correlates well with the N* binding energy,[5] this represents a BEP plot with the x-axis giving a surrogate measure of the reaction energy for reduction, and a direct measure of the reaction energy for dissociation. The BEP relationship holds very well for $N_2$ dissociation on (111) surfaces of FCC metals.[32] The values calculated here are in good agreement with previously reported $N_2$ dissociation barriers on similar surfaces.[32–35] For the FCC metals, the $N_2$ dissociation barriers range from 2.03 eV for the Ni(111) surface to 4.36 eV for the Cu(111) surface. Fe and Ru bind N* stronger
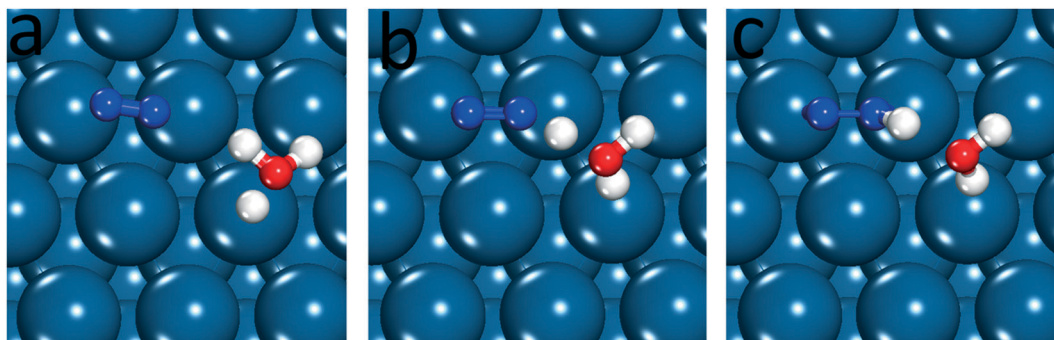
176 | *Catal. Sci. Technol.*, 2019, **9**, 174–181

This journal is © The Royal Society of Chemistry 2019

**Fig. 1** Equilibrium and transition states for $N_2$ reduction to $N_2H^*$ on Pt(111), (a) initial state, (b) transition state and (c) final state.

such that the $N_2$ dissociation barrier is 1.72 eV on the Ru(0001) surface and 0.59 eV on the Fe(110) surface.

The BEP relationship for $N_2$ reduction does not hold well, as the barriers show only a rough linear correlation with the nitrogen binding energy for FCC metals. For FCC metals, reductive $N_2$ adsorption barriers range from 1.36 eV on the Rh(111) surface to 2.57 eV on the Cu(111) surface at 0 V-RHE. For the FCC metals, the $N_2$ dissociation barrier is significantly higher than the reductive $N_2$ adsorption barrier at 0 V-RHE. The smallest difference is on the Rh(111) surface where the $N_2$ dissociation barrier is 1.05 eV higher. Decreasing the potential will further decrease the reductive $N_2$ adsorption barrier (via eqn (8)), and, therefore, the reductive $N_2$ adsorption barrier is lower than the dissociation barrier at all

NRR conditions on all these FCC(111) surfaces. We reach the same conclusion based on reaction energies alone,[4] that ambient condition NRR will follow an associative mechanism. This conclusion must be qualified by noting that the results presented consider only low index facets, whereas $N_2$ dissociation would be more facile on stepped surfaces. As we also have not considered $N_2H^*$ formation at steps, the results presented here are only directly applicable to the low index surfaces considered.

For Ru(0001) surface, the $N_2$ dissociation barrier is 0.08 eV higher than the reductive $N_2$ adsorption barrier at 0 V-RHE. Alternatively, for Fe(110) surface, the $N_2$ dissociation barrier is 0.22 eV lower than the reductive $N_2$ adsorption barrier at 0 V-RHE. Reductive overpotentials will lead to preferential initial reduction rather than dissociation, though the two mechanisms will be competitive at typical NRR conditions.

As the $N_2$ reduction barriers do not correlate well with N* binding energies, we considered a more direct BEP correlation with the product formation $N_2H^*$ energy. Fig. 3 shows a more reliable correlation for the FCC metals ($R^2 = 0.83$ compared to 0.66 using N* binding energies). We use $N_2H^*$ binding energy, rather than N* binding energy, as our descriptor for predicting activation barriers due to this stronger correlation. The non-FCC Ru(0001) and Fe(110) surfaces show considerable deviation relative to the FCC(111) trend.

### 3.2. NH* to $NH_2^*$ reduction and kinetic trade-offs in NRR catalyst optimization

Montoya et al. calculated the $\Delta G$ of all NRR elementary steps on (111) and (211) surfaces of many transition metals.[4] Based on the elementary step thermodynamics, they suggest that most late transition metals were limited by the initial reductive hydrogenation of nitrogen on the surface, in agreement with the large barriers for this step reported in the previous section. Elementary step thermodynamics suggested that NRR might be limited by hydrogenation of NH* on strongly binding transition metals:

$$NH^* + H_2O + H^+ + e^- \rightarrow NH_2^* + H_2O \qquad (16)$$

We therefore determined the activation barrier for the NH* reduction. Fig. 4 illustrates the preferred adsorption
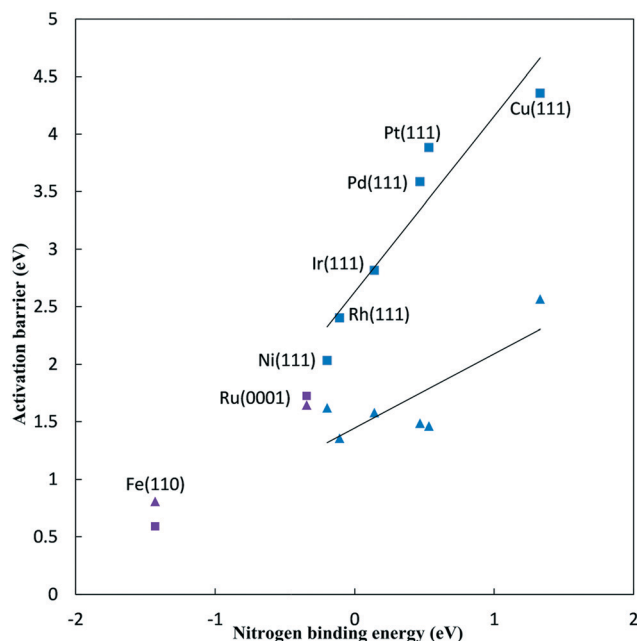


**Fig. 2** Activation barriers for initial $N_2$ activation on late transition metal surfaces at 0 V RHE, plotted against the N* adsorption energy to the same surface. ■ – $N_2$ dissociation barriers, ▲ – $N_2$ to $N_2H^*$ reduction barriers, blue – FCC(111) metal surfaces, purple – Fe(110) and Ru(0001) surfaces. Linear best fits are shown for FCC metals, $Ga_3$ = 1.53 ($N_2$ binding energy) + 2.63 eV ($R^2 = 0.89$) for dissociation and $Ga_1$ = 0.65 ($N_2$ binding energy) + 1.45 eV ($R^2 = 0.66$) for reduction.
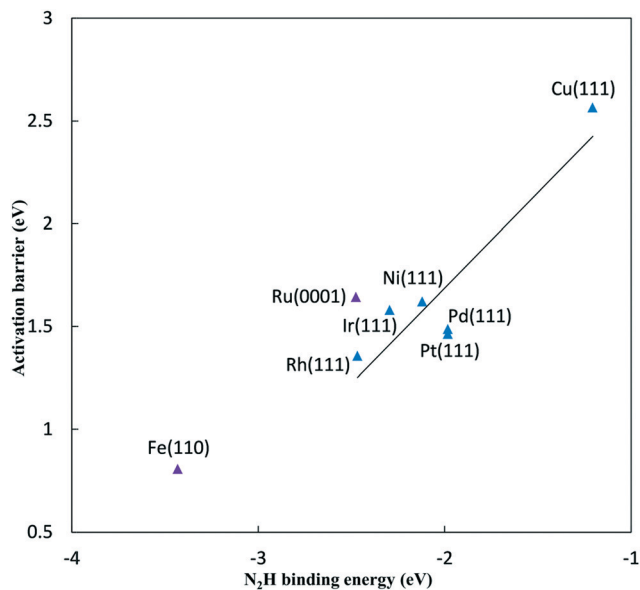
**Fig. 3** Activation barriers for $N_2$ to $N_2H^*$ reduction on late transition metal surfaces at 0 V-RHE, plotted against $N_2H^*$ binding energy to the same surface. Blue – FCC(111) metal surfaces, purple – Fe(110) and Ru(0001) surfaces. Linear best fit are shown for FCC metals, $Ga_1 = 0.93$ ($N_2H$ binding energy) + 3.55 eV ($R^2 = 0.83$).
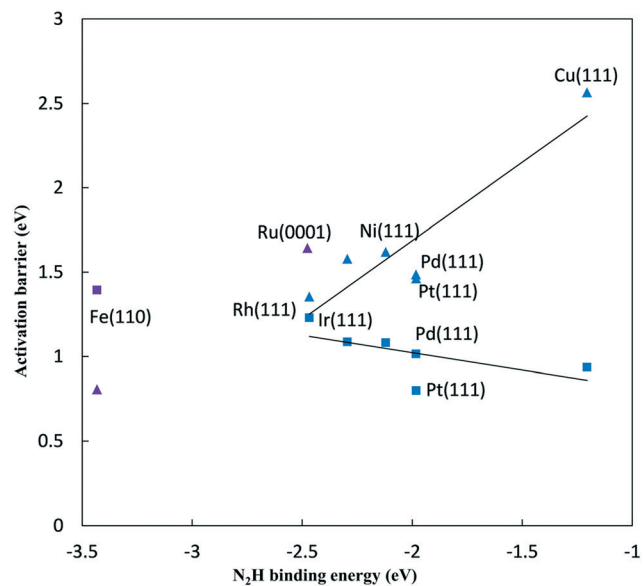


**Fig. 5** Activation barriers for $N_2$ and $NH^*$ reduction on late transition metal surfaces at 0 V-RHE, plotted against $N_2H^*$ binding energy to the same surface. ▲ – $N_2$ to $N_2H^*$ reduction barriers, ■ – $NH^*$ to $NH_2^*$ reduction barriers, blue – FCC(111) metal surfaces, purple – Fe(110) and Ru(0001) surfaces. Linear best fit are shown for fcc metals, $Ga_1 = 0.93$ ($N_2H$ binding energy) + 3.55 eV ($R^2 = 0.83$) for $N_2$ reduction and $Ga_2 = -0.21$ ($N_2H$ binding energy) + 0.61 eV ($R^2 = 0.37$) for $NH^*$ reduction.

configuration of the initial state, transition state and final state on the Pt(111) surface.

On Pt(111) the dissociating O–H bond of $H_2O$ is extended from 0.98 Å in the initial state to 1.02 Å in the transition state. The forming N–H bond distance is 1.76 Å as the H is shared between O and N at the transition state. Similarly, the transition state for NH* hydrogenation was located for the same surfaces used in the previous section. The NH* reduction barriers are plotted along with the $N_2^*$ reduction barriers at 0 V-RHE in Fig. 5. All non-electrochemical (hydrogenation) barriers and $U^0$ values are given in the ESI.†

The reductive $N_2$ adsorption and NH* reduction barriers are plotted against the $N_2H^*$ binding energy at 0 V-RHE in Fig. 5. For FCC metals, NH* reduction barriers range from 0.8 eV for the Pt(111) surface to 1.23 eV for the Rh(111) surface at 0 V-RHE ($R^2 = 0.37$). Fe(110) has a large barrier for

NH* reduction as iron binds NH* strongly. Surfaces with stronger $N_2H^*$ binding, generally, have higher barriers for NH* reduction This is in contrast with the $N_2H^*$ formation, such that the slopes of barriers for $N_2$ reduction against the $N_2H^*$ binding (0.93) is positive and sharper than that for NH* reduction (−0.21).

For all FCC surfaces, the reductive $N_2$ adsorption has a higher barrier than NH* reduction and, therefore, limits the overall NRR rate. This is consistent with conclusions based on elementary step thermodynamics.[4]

Initial $N_2$ reduction and NH* reduction have been considered rate limiting steps for the NRR based on the thermodynamic equilibrium data and limiting potentials. By considering these steps as kinetic rate limiting steps for the NRR, Fig. 5 represents a kinetic volcano for the NRR. Though the data in this figure are barriers at 0 V-RHE, both data sets
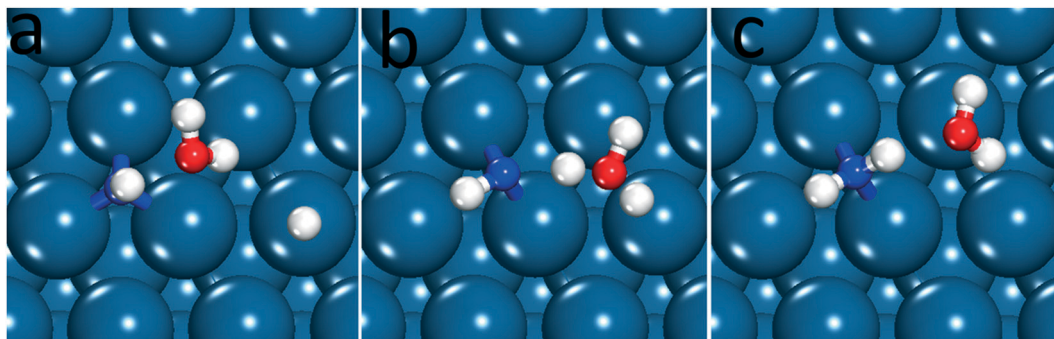


**Fig. 4** Reaction path for NH* hydrogenation on the Pt(111) surface, (a) initial state, (b) transition state and (c) final state.

would move down in barrier equivalently if potential was lowered, provided both steps had the same symmetry coefficient. The rate limiting step is determined by the higher barrier between $N_2$ and NH* reduction steps. Therefore, the crossing point of the kinetic volcano would optimize the NRR rate. For the FCC metals, these lines do not cross suggesting that a stronger binding transition metal is required to lower the effective barrier on FCC metals. This is consistent with the purely "thermodynamic volcano", which indicates that the optimal catalyst bind slightly stronger to reaction intermediates.[4] Based on the thermodynamic volcano, this crossing point falls between ruthenium and rhenium which both bind stronger to reaction intermediates than the FCC(111) surfaces we considered. Alternatively, if we consider the Fe(110) surface in the correlations, the crossing point falls between ruthenium and rhodium on the right and iron on the left side suggesting that an optimal transition metal binds stronger than ruthenium and rhodium and weaker than iron to the reaction intermediates. However, data scatter from the correlations and error associated with the reaction path are significant, and if we examine the DFT barriers directly rather than the correlations, it would be difficult to differentiate between ruthenium, iron, rhodium and even platinum. Kinetic volcano and elementary thermodynamics are in qualitative agreement and both suggest that for strong binding catalysts, such as iron, the reaction is limited by NH* reduction, and weak binding catalysts are limited by initial $N_2$ to $N_2H$* reduction. If we assume that data scattered from the correlations are less reliable than the correlations themselves, we conclude that an optimal catalyst binds $N_2H$* stronger than ruthenium and weaker than iron. Alloying to weaken $N_2H$* binding on Fe might reduce the overpotentials required for the $N_2$ reduction.

The kinetic volcano suggests that the barrier for the rate limiting step at 0 V-RHE will be 1.15 eV on the optimal catalyst, which is a significant barrier in line with the low NRR activity on all tested metals at room temperature. The effective NRR barriers range from 1.36 eV on the Rh(111) surface to 2.57 eV on the Cu(111) surface at 0 V-RHE, suggesting that none of these transition metals can effectively convert nitrogen to ammonia at 0 V-RHE (Table 1). Therefore, large overpotentials are required to produce ammonia on all these transition metals. Decreasing the electrode potential reduces the effective NRR barrier, with the barrier decreasing by 0.5

eV if the voltage is lowered by 1 V if a $\beta$ of 0.5 is assumed. The overpotential required to decrease the effective NRR barrier to a reasonable value of 0.4 eV is calculated from eqn (9) and is presented in Table 2. The required overpotential for $N_2$ reduction varies from 1.91 V for Rh(111) surface to 4.33 V for Cu(111) surface. These large overpotentials suggest that nitrogen reduction on all these surfaces is very inefficient and energy intensive. Experimental results also show that NRR has a low rate at small overpotentials over various transition metal surfaces.[1,15,36]

### 3.3. Hydrogen evolution reaction (HER) competition with $N_2$ reduction

In addition to large overpotentials and low catalytic activity, the NRR reaction is challenged by poor selectivity due to the competing HER. The potential dependent proton adsorption barriers and hydrogen evolution barriers (Tafel reaction) are calculated in order to quantify the relative barriers to nitrogen reduction.

**3.3.1. Hydrogen adsorption on low index surfaces of late transition metals.** We next consider the proton adsorption barrier on different catalytic surfaces. Higher proton adsorption barriers will reduce the hydrogen evolution rate. Proton adsorption barriers were evaluated and converted to potential dependent barriers using eqn (8). Generally, the approximated transition states located with a single water resemble an $H_3O^{\delta+}$ species bound to the surface. Though we report an activation barrier for Cu(111), the located transition state did not have an imaginary frequency and is instead an intermediate state along the proton adsorption path. The adsorption barrier, therefore, is expected to be slightly higher than the number reported here for the Cu(111) surface. Table 2 presents the activation free energy of proton adsorption over transition metals at 0 V-RHE. The proton adsorption barriers on all metals are considerably lower than elementary NRR barriers. Our approach of treating the Volmer step barriers using a single water molecule to transfer the proton between sites is clearly approximate, likely overestimating the barriers by 0.2–0.4 eV. Qualitatively, however this approach matches that used for NRR to provide comparable values that confirm lower HER barriers. We also find that trends across metals meet expectations, with the small barrier of 0.25 eV at 0 V-RHE in agreement with the observed small overpotential

**Table 1** Limited step activation barriers (at 0 V-RHE) and estimated overpotentials required for each surface to provide a practical NRR rate (barrier less than 0.4 eV)

| Surface | 0 V-RHE barrier (eV) | Overpotential (V-RHE) |
|---|---|---|
| Pt(111) | 1.46 | −2.13 |
| Ir(111) | 1.58 | −2.36 |
| Rh(111) | 1.36 | −1.91 |
| Cu(111) | 2.57 | −4.33 |
| Ni(111) | 1.62 | −2.44 |
| Pd(111) | 1.49 | −2.17 |
| Fe(110) | 1.39 | −1.99 |

**Table 2** Estimated hydrogen adsorption barriers (eV) ($H^+ + e^- + H_2O + *$ → H* + $H_2O$) over transition metal surfaces

| Surface | $G_{a,H}$ (eV) at 0 V RHE |
|---|---|
| Pt(111) | 0.25 |
| Ir(111) | 0.78 |
| Rh(111) | 0.94 |
| Cu(111) | 1.13 |
| Ni(111) | 0.98 |
| Pd(111) | 0.76 |
| Ru(0001) | 1.06 |
| Fe(110) | 1.08 |

for HER on Pt electrodes.[37] Low barriers for H* formation are suggestive both of fast HER rates and that H* will successfully compete with $N_2$ reduction intermediates for surface sites.

**3.3.2. $H_2$ associative desorption barriers on late transition metals.** The $H_2$ associative desorption barriers (Tafel step) were calculated using the CI-NEB method, and are plotted along with NRR barriers in Fig. 6 at 0 V-RHE. The hydrogen binding energy was used as a descriptor in this figure because hydrogen evolution barriers correlate better with hydrogen binding energies, though the correlation of NRR barriers with this descriptor is clearly poor. For all transition metals except copper, the HER transition state free energies were about 0–0.1 eV higher than the free energy of final states. This is consistent with previous studies finding that the hydrogen adsorption barrier is negligible or small for these transition metals.[38–42] We did not consider Heyrovsky barriers for the $H_2$ formation step as all Tafel barriers were low, such that the approximate barrier method used herein would simply conclude that Heyrovsky barriers are also similar to reaction free energies. As observed in Fig. 6, the Tafel reaction barriers are all considerably lower than the corresponding NRR barriers. Decreasing the electrode potential lowers the NRR barriers, though this would also lower the barriers for the Volmer step, allowing H* to outcompete NRR intermediates for surface sites. The resultant higher coverage of H* at low potentials would also likely lead to lower Tafel step barriers. For example, we calculated the hydrogen evolution

barrier on Pt(111) surface with a 10/9 monolayer of hydrogen at the initial state. Increasing the initial state surface coverage from 2/9 monolayer to 10/9 monolayer lowered the Tafel barrier from 0.67 eV to 0.31 eV (see Fig. S5 in the ESI† for images of the 10/9 ML structures). Both Volmer and Tafel steps of HER are found to have considerably lower barriers than the NRR steps at reasonable NRR overpotentials, in agreement with the low NRR selectivity observed on these catalysts.

## 4. Summary and conclusions

Previous DFT studies have suggested rate limiting steps and reaction paths for NRR on late transition metals, but did so based on elementary step thermodynamics without explicit consideration of potential dependent barriers for electrochemical steps. Elementary activation barriers were reported for initial $N_2$ reduction, $N_2$ dissociative adsorption, reduction of surface bound NH*, and the Volmer and Tafel steps of HER. Low index surfaces of late transition metals were considered. A "kinetic volcano" was developed for nitrogen reduction over (111) surfaces of FCC metals. The qualitative conclusions reached based on elementary kinetics match those based on elementary step thermodynamics – that weakly binding metals are limited by initial $N_2$ activation and strongly binding metals are limited by reduction of surface bound $NH_x^*$ species. Kinetic barriers suggest large overpotentials for NRR, suggesting low activity and high overpotentials of all late transition metals (or at least their low index facets). NRR barriers are greater than 1 eV on all surfaces considered, significantly exceeding those for HER calculated with the same approach. The low activity due to high NRR barriers and low selectivity due to lower HER barriers demonstrate the extreme challenge in developing active and selective NRR electrocatalysts.

## Conflicts of interest

There are no conflicts to declare.

## Acknowledgements

**Fig. 6** Activation barriers for $N_2$ and NH* reduction and hydrogen evolution on late transition metal surfaces at 0 V-RHE, plotted against hydrogen binding energy to the same surface. ▲ – $N_2$ to $N_2$H* reduction barriers, ■ – NH* to $NH_2^*$ reduction barriers, ● – HER barriers, blue – FCC(111) metal surfaces, purple – Fe(110) and Ru(0001) surfaces. Linear best fit are shown for FCC metals, $Ga_1$ = 2.54 (hydrogen binding energy) + 2.86 eV ($R^2$ = 0.59) for $N_2$ reduction, $Ga_2$ = −0.38 (hydrogen binding energy) + 0.85 eV ($R^2$ = 0.12) for NH* reduction and $Ga_{H_2}$ = −0.56 (hydrogen binding energy) + 0.40 eV ($R^2$ = 0.55) for HER.

## References

1 J. N. Renner, L. F. Greenlee, K. E. Ayres and A. M. Herring, *Electrochem. Soc. Interface*, 2015, **24**, 51–57.
2 J. G. Chen, R. M. Crooks, L. C. Seefeldt, K. L. Bren, R. M. Bullock, M. Y. Darensbourg, P. L. Holland, B. Hoffman, M. J.
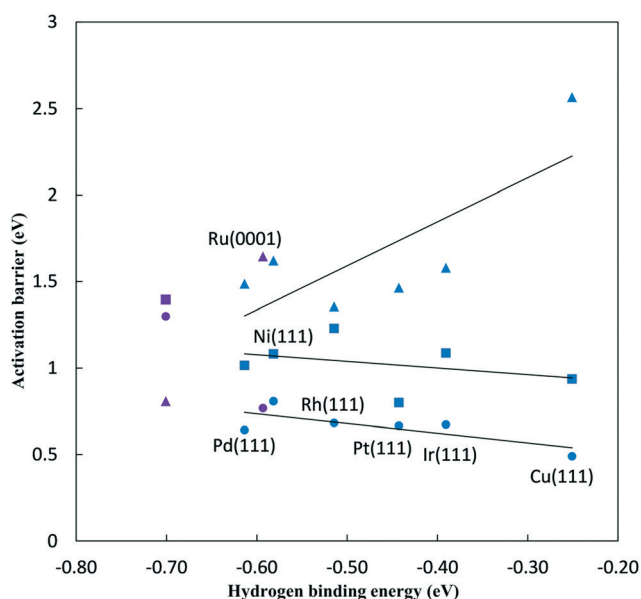
Janik, A. K. Jones, M. G. Kanatzidis, P. King, K. M. Lancaster, S. V. Lymar, P. Pfromm, W. F. Schneider and R. R. Schrock, *Science*, 2018, **360**, 6391.

3  S. L. Foster, S. I. P. Bakovic, R. D. Duda, S. Maheshwari, R. D. Milton, S. D. Minteer, M. J. Janik, J. N. Renner and L. F. Greenlee, *Nat. Catal.*, 2018, **1**, 490–500.

4  J. H. Montoya, C. Tsai, A. Vojvodic and J. K. Nørskov, *ChemSusChem*, 2015, **8**, 2180–2186.

5  E. Skulason, T. Bligaard, S. Gudmundsdottir, F. Studt, J. Rossmeisl, F. Abild-Pedersen, T. Vegge, H. Jonsson and J. K. Norskov, *Phys. Chem. Chem. Phys.*, 2012, **14**, 1235–1245.

6  R. Lan, J. T. S. Irvine and S. Tao, *Sci. Rep.*, 2013, **3**, 1145.

7  S. Licht, B. Cui, B. Wang, F.-F. Li, J. Lau and S. Liu, *Science*, 2014, **345**, 637–640.

8  G. Qing, R. Kikuchi, S. Kishira, A. Takagaki, T. Sugawara and S. T. Oyama, *J. Electrochem. Soc.*, 2016, **163**, E282–E287.

9  G.-F. Chen, S. Ren, L. Zhang, H. Cheng, Y. Luo, K. Zhu, L.-X. Ding and H. Wang, *Small Methods*, 2018, 1800337.

10  X. Cui, C. Tang and Q. Zhang, *Adv. Energy Mater.*, 2018, **8**, 1800369.

11  R. Manjunatha and A. Schechter, *Electrochem. Commun.*, 2018, **90**, 96–100.

12  R. D. Milton, S. Abdellaoui, N. Khadka, D. R. Dean, D. Leech, L. C. Seefeldt and S. D. Minteer, *Energy Environ. Sci.*, 2016, **9**, 2550–2554.

13  X. Yang, J. Nash, J. Anibal, M. Dunwell, S. Kattel, E. Stavitski, K. Attenkofer, J. G. Chen, Y. Yan and B. Xu, *J. Am. Chem. Soc.*, 2018, **140**, 13387–13391.

14  R. L. Cook and A. F. Sammells, *Catal. Lett.*, 1988, **1**, 345–349.

15  V. Kordali, G. Kyriacou and C. Lambrou, *Chem. Commun.*, 2000, 1673–1674, DOI: 10.1039/B004885M.

16  S. Grayer and M. Halmann, *J. Electroanal. Chem. Interfacial Electrochem.*, 1984, **170**, 363–368.

17  S. Back and Y. Jung, *Phys. Chem. Chem. Phys.*, 2016, **18**, 9161–9166.

18  A. L. Garden and E. Skúlason, *J. Phys. Chem. C*, 2015, **119**, 26554–26559.

19  L. Rao, X. Xu and C. Adamo, *ACS Catal.*, 2016, **6**, 1567–1577.

20  S. Maheshwari, G. Rostamikia and M. J. Janik, *J. Chem. Phys.*, 2018, **150**, 041708.

21  G. Kresse and J. Furthmuller, *Comput. Mater. Sci.*, 1996, **6**, 15–50.

22  G. Kresse and J. Furthmuller, *Phys. Rev. B: Condens. Matter Mater. Phys.*, 1996, **54**, 11169–11186.

23  G. Kresse and J. Hafner, *Phys. Rev. B: Condens. Matter Mater. Phys.*, 1993, **47**, 558–561.

24  J. P. Perdew and Y. Wang, *Phys. Rev. B: Condens. Matter Mater. Phys.*, 1992, **45**, 13244.

25  J. P. Perdew, K. Burke and M. Ernzerhof, *Phys. Rev. Lett.*, 1996, **77**, 3865–3868.

26  H. J. Monkhorst and J. D. Pack, *Phys. Rev. B: Solid State*, 1976, **13**, 5188–5192.

27  G. Henkelman and H. Jonsson, *J. Chem. Phys.*, 2000, **113**, 9978–9985.

28  G. Henkelman, B. P. Uberuaga and H. Jonsson, *J. Chem. Phys.*, 2000, **113**, 9901–9904.

29  G. Rostamikia, A. J. Mendoza, M. A. Hickner and M. J. Janik, *J. Power Sources*, 2011, **196**, 9228–9237.

30  A. Bard, L. Faulkner, A. J. Bard and L. R. Faulkner, *Electrochemical Methods: Fundamentals and Applications*, Wiley, New York, 2001, p. 2002.

31  A. C. Lausche, A. J. Medford, T. S. Khan, Y. Xu, T. Bligaard, F. Abild-Pedersen, J. K. Nørskov and F. Studt, *J. Catal.*, 2013, **307**, 275–282.

32  T. R. Munter, T. Bligaard, C. H. Christensen and J. K. Nørskov, *Phys. Chem. Chem. Phys.*, 2008, **10**, 5202–5206.

33  C. H. Christensen and J. K. Nørskov, *J. Chem. Phys.*, 2008, **128**, 182503.

34  J. A. Herron, P. Ferrin and M. Mavrikakis, *J. Phys. Chem. C*, 2015, **119**, 14692–14701.

35  J. K. Nørskov, T. Bligaard, A. Logadottir, S. Bahn, L. B. Hansen, M. Bollinger, H. Bengaard, B. Hammer, Z. Sljivancanin, M. Mavrikakis, Y. Xu, S. Dahl and C. J. H. Jacobsen, *J. Catal.*, 2002, **209**, 275–278.

36  R. Lan and S. Tao, *RSC Adv.*, 2013, **3**, 18016–18021.

37  N. M. Marković, B. N. Grgur and P. N. Ross, *J. Phys. Chem. B*, 1997, **101**, 5405–5413.

38  K. Nobuhara, H. Kasai, W. A. Diño and H. Nakanishi, *H2 dissociative adsorption on Mg, Ti, Ni, Pd and La Surfaces*, 2004.

39  C. T. Rettner, H. A. Michelsen and D. J. Auerbach, *J. Chem. Phys.*, 1995, **102**, 4625–4641.

40  W. Dong, G. Kresse and J. Hafner, *J. Mol. Catal. A: Chem.*, 1997, **119**, 69–76.

41  N. B. Arboleda and H. Kasai, *Surf. Interface Anal.*, 2008, **40**, 1103–1107.

42  W. Dong and J. Hafner, *H2 dissociative adsorption on Pd(111)*, 1997.

This journal is © The Royal Society of Chemistry 2019

*Catal. Sci. Technol.*, 2019, **9**, 174–181 | 181